# Faster-than-realtime inverse simulation method for tiltrotor handling qualities investigation

Ye Yuan [a],*, Douglas Thomson [b], David Anderson [b]

[a] *Swansea University, Swansea, Wales, SA1 8EN, United Kingdom*
[b] *University of Glasgow, Glasgow, Scotland, G12 8QQ, United Kingdom*

A B S T R A C T

The tiltrotor aircraft has unique flight dynamics characteristics because of the extensive aerodynamic interference and the unique control strategy. Inverse simulation offers an opportunity to study a vehicle's performance during manoeuvring flights. In this paper, an improved inverse simulation method is developed with an Automatic Differentiation (AD) approach embedded in the code based on the verified flight dynamics model of the tiltrotor aircraft. The AD algorithm would accelerate the computational rate of the inverse simulation process and make it achieve faster-than-realtime capability. Then, the XV-15 tiltrotor's control inputs and flight states encountered during a pop-up manoeuvre are investigated using this AD-augmented inverse simulation method, and the real-time capability of this method is also evaluated. The results indicate that the proposed method guarantees both accuracy and faster-than-realtime calculation performance. Lastly, the tiltrotor's manoeuvrability is assessed by executing this manoeuvre in different flight states and manoeuvre settings. Lastly, an envelope involving the velocity and nacelle incidence angle is calculated to indicate the safety region to achieve this pop-up manoeuvre.

© 2022 The Author(s). Published by Elsevier Masson SAS. This is an open access article under the CC BY license (http://creativecommons.org/licenses/by/4.0/).

## 1. Introduction

The tiltrotor aircraft has drawn extensive research attention as it has the capability to combine the advantages of the fixed-wing aircraft and the helicopter, making it simultaneously possess the capacity to hover and perform high-speed flight [1–3].

However, the manoeuvrability of this aircraft configuration is complicated. Firstly, the nacelle of this aircraft needs to tilt forward from helicopter mode to aircraft mode in order to achieve higher forward speeds. The stability and controllability in this regime are dramatically modified [4–6], which may degrade its manoeuvrability [7]. The interaction between the rotor wake and other parts of the vehicle alters the aerodynamic forces and consequently influences the flight dynamics characteristics during manoeuvring flight. Besides, both helicopter and fixed-wing aircraft control inputs are integrated into the tiltrotor aircraft [8–10], and relevant control allocations will determine the control power, significantly affecting the manoeuvrability.

Inverse simulation is a widely used method to analyse the manoeuvrability of rotorcraft and tiltrotor aircraft [11–13]. It is a technique by which the control actions can be calculated for an aircraft to execute a given manoeuvre. This method can be seen as a nonlinear equation solution process. The numerical differentiation process is usually utilised to obtain the Jacobian matrix for the equation solution, and consequently, the flight dynamics model has to be called several times [14]. This makes the computational time relatively high and difficult to accelerate. The automatic differentiation (AD) method is a potential approach to improve the efficiency of inverse simulation [15,16]. Compared to the traditional numerical differentiation method, the automatic differentiation algorithm avoids repeatedly calling the flight dynamics model, reducing the calculation duration. Besides that, the automatic differentiation method can enhance the accuracy of the results by avoiding any round-off error. This method has been widely utilised for helicopter and fixed-wing aircraft CFD calculations to optimise geometry and analyse rotor aerodynamic stability [17,18]. In this paper, the application of automatic differentiation to inverse simulation is described.

There has been much research to date related to flight dynamics analysis for tiltrotor aircraft. A series of wind-tunnel experiments were carried out focusing on the XV-15 tiltrotor aircraft [19–23]. In this research, the trim and stability characteristics of the tiltrotor aircraft were assessed, and a simulation model was built (Generic TiltRotor Simulation program, known as GTRS) based

* Corresponding author.
*E-mail address:* ye.yuan@swansea.ac.uk (Y. Yuan).

## Nomenclature

| | | |
|---|---|---|
| $A_1$ | lateral cyclic pitch | deg |
| $B_{1L}$, $B_{1R}$ | longitudinal cyclic pitches of left and right rotors | deg |
| $\boldsymbol{J}$ | Jacobian matrix | |
| $V_{f,i}$ | initial forward speed | m/s |
| $X_{col}$ | collective pitch controller | deg |
| $X_{LN}$ | longitudinal control input | deg |
| $X_{LT}$ | lateral control input | deg |
| $X_{PD}$ | pedal control input | deg |
| $\boldsymbol{e}$ | error vector | |
| $h$ | given height in manoeuvre | m |
| $m$ | solution step at every time point | |
| $p$, $q$, $r$ | angular velocities | rad/s |
| $t$ | time | s |
| $t_k$ | time step | |
| $t_m$ | time to complete the manoeuvre | s |
| $\bar{t}$ | normalised time cost | |
| $t_{cal}$, $t_{real}$ | calculation time cost and corresponding real-time period | s |
| $tol$ | tolerance | |
| $s$ | longitudinal distance | m |
| $\boldsymbol{u}$ | control vector of the tiltrotor aircraft | deg |
| $u$, $v$, $w$ | velocities in body axis | m/s |
| $v_{10}$, $v_{1c}$, $v_{1s}$ | induced velocities on the left rotor disk | m/s |
| $v_{20}$, $v_{2c}$, $v_{2s}$ | induced velocities on the right rotor disk | m/s |
| $\boldsymbol{x}$ | state vector of the tiltrotor aircraft | |
| $x_e$, $y_e$, $z_e$ | displacements in the earth coordinate | m |
| $\boldsymbol{y}$ | manoeuvre trajectory | |
| $\boldsymbol{y}_{des}$ | desired manoeuvre path | |
| $\theta$, $\varphi$, $\psi$ | attitude angles | deg |
| $\theta_{0L}$, $\theta_{0R}$ | collective pitches of the left and right rotors | |
| $\beta_m$ | nacelle incidence angle (deg) - 0 deg represents the helicopter mode | |
| $\beta_{10}$, $\beta_{1c}$, $\beta_{1s}$ | coning, sine and cosine components of the left rotor flapping motion | deg |
| $\beta_{20}$, $\beta_{2c}$, $\beta_{2s}$ | coning, sine and cosine components of the right rotor flapping motion | deg |
| $\delta_{B1}$ | pre-determined longitudinal cyclic angle | deg |
| $\delta_e$, $\delta_r$, $\delta_a$ | deflections of elevator, rudder, and aileron | deg |

on these wind tunnel experiments. The stability and controllability derivatives were also tested, showing that the flight dynamics characteristics of the tiltrotor aircraft are highly dependent on the nacelle incidence angle and forward speed, implying an essential coupling between the nacelle position and vehicle manoeuvrability. Other researchers [24,25] evaluated the manoeuvrability of the tiltrotor aircraft based on the numerical optimisation method and stability & controllability matrices. However, these methods focus more on performance investigation and trajectory calculation rather than flight dynamics investigation.

Inverse simulation has been developed steadily in recent years, including its accuracy and feasibility improvement. Rutherford [26,27] combined the inverse simulation method with an individual blade model using the periodic trim and response algorithm, further enhancing its accuracy in rotor aerodynamics calculation. Cameron [28] introduced a pilot model into the inverse simulation method. Thus, the pilot-induced oscillation is included in the inverse simulation results. Wu [29] developed a general method for inverse simulation with the flight control system online to solve the coupling problem between pilot controls and flight control system outputs.

However, calculation speed is still a critical challenge for the inverse simulation method [30,31]. Computational time requirement impedes inverse simulation for complex models of the type essential for the tiltrotor aircraft. The real-time capability of the inverse simulation has the potential to extend its applications towards control system design and autonomous system development. Additionally, suppose the inverse simulation has the real-time or even faster-than-realtime capability. In that case, it can be directly utilised to form the auto-pilot system for tiltrotor aircraft.

In light of the preceding discussion, this article first describes the construction of the flight dynamics model of the tiltrotor aircraft briefly. Then, the automatic differentiation embedded inverse simulation technique is developed. The pop-up manoeuvre is utilised here to test the performance of the improved inverse simulation method and investigate the manoeuvrability of the tiltrotor aircraft. Then, the control input and flight status during the pop-up manoeuvre are calculated and investigated, and the calculation efficiency of this improved inverse simulation method is also assessed.

## 2. Methodology

The methodology section has four components: the tiltrotor flight dynamics model, the inverse simulation method, the automatic differentiation algorithm, and the pop-up manoeuvre description.

### 2.1. Flight dynamics model

Tiltrotor aircraft can be seen as a combination between the helicopter and fixed-wing aircraft. It is symmetric with respect to the X-Z body axis, and its twin rotors are counter-rotating. Thus, the longitudinal and lateral-yawing channels are decoupled. The flight dynamics model used in this research is based on the XV-15 tiltrotor aircraft, which contains five components: rotor model, pylon & wing model, vertical fin model, horizontal tail model, and fuselage model. The rotor model is constructed using an individual blade method [32]. The aerofoil aerodynamic model is based on the fitting polynomials provided by the GTRS report [20]. These polynomials consider the stall and compressibility effects. A fixed-wake method is utilised to calculate the aerodynamics interference between rotors and the aerodynamics interaction between rotor wakes and other components, such as wing and tailplanes. The rotor model features the Pitt-Peters dynamic inflow model to estimate the induced velocity on the rotor disk [33]. The modelling methods of the other components, including the fuselage, wing & pylon, and tailplane, use the results from reference [34], which is based on wind tunnel experiment results. The detailed modelling process and validation (trim and stability verifications) can be found in reference [35].

Therefore, the 6 Degrees of Freedom (DOF) flight dynamics model of the tiltrotor aircraft is presented taking the nonlinear form of

$$\dot{\boldsymbol{x}} = \boldsymbol{f}(\boldsymbol{x}, \boldsymbol{u}, t) \tag{1}$$

where $\boldsymbol{x}$ is the state vector, including the vehicle velocities in body axis ($u$, $v$, $w$), angular velocities ($p$, $q$, $r$), attitude angles ($\theta$, $\varphi$, $\psi$), blade flapping motions ($\beta_{10}$, $\beta_{1c}$, $\beta_{1s}$, $\beta_{20}$, $\beta_{2c}$, $\beta_{2s}$), and induced velocities ($v_{10}$, $v_{1c}$, $v_{1s}$, $v_{20}$, $v_{2c}$, $v_{2s}$). The corresponding sign conventions of these parameters are based on the definition shown in reference [36]. $\boldsymbol{u}$ is the control vector, which contains

the collective pitch controller, the longitudinal and lateral control inputs, and the pedal control input; $t$ is the response time.

The control strategy of the tiltrotor aircraft is unique, as it combines the control inputs of both the helicopter and the fixed-wing aircraft. Based on the XV-15 tiltrotor aircraft [34], the control strategies of different controllers are shown below

$$\theta_{0L} = (\frac{\partial \theta_0}{\partial X_{col}})X_{col} + (\frac{\partial \theta_0}{\partial X_{LT}})X_{LT} \tag{2}$$

$$\theta_{0R} = (\frac{\partial \theta_0}{\partial X_{col}})X_{col} - (\frac{\partial \theta_0}{\partial X_{LT}})X_{LT} \tag{3}$$

$$A_1 = 0 \tag{4}$$

$$B_{1L} = (\frac{\partial B_1}{\partial X_{LN}})X_{LN} - (\frac{\partial B_1}{\partial X_{PD}})X_{PD} + \delta_{B1}(1 - \cos(\beta_m)) \tag{5}$$

$$B_{1R} = (\frac{\partial B_1}{\partial X_{LN}})X_{LN} + (\frac{\partial B_1}{\partial X_{PD}})X_{PD} + \delta_{B1}(1 - \cos(\beta_m)) \tag{6}$$

$$\delta_e = (\frac{\partial \delta_e}{\partial X_{LN}})X_{LN} \tag{7}$$

$$\delta_r = (\frac{\partial \delta_r}{\partial X_{PD}})X_{PD} \tag{8}$$

$$\delta_a = (\frac{\partial \delta_a}{\partial X_{LT}})X_{LT} \tag{9}$$

where $\theta_{0L}$ and $\theta_{0L}$ are the collective pitches of left and right rotors, respectively; $X_{col}$ is the collective pitch controller; $X_{LT}$ denotes the lateral control input; $A_1$ represents the lateral cyclic pitch; $B_{1L}$ and $B_{1R}$ denote the longitudinal cyclic pitches of the left and right rotors; $X_{LN}$ is the longitudinal control input; $X_{PD}$ is the pedal control input; $\delta_{B1}$ is the pre-determined longitudinal cyclic angle, which is set to -1.5 deg in the XV-15 tiltrotor aircraft; $\beta_m$ is the nacelle incidence angle, which 0 deg represents the helicopter mode. $\delta_e$, $\delta_r$, and $\delta_a$ represent the deflections of elevator, rudder, and aileron. By changing the parameters in Eqs. (5)-(7), the longitudinal cyclic pitches are phased out in the aircraft mode, and the elevator deflection is used to provide all the control power in the pitching channel at this flight range.

### 2.2. Inverse simulation method

Inverse simulation is a widely used method for the manoeuvrability analysis of helicopter and fixed-wing aircraft. As the logic of this method has been comprehensively documented in the literature [37–39], only a brief introduction will be provided here.

The so-called integration inverse simulation is utilised, readily available when the flight dynamics model has been constructed. The first step in the inverse simulation is to determine the control inputs at the starting point. This starting point usually refers to the trimmed level flight state at a given velocity. The next step is to define the manoeuvre trajectory. At each time step, a matrix $\mathbf{y}_{des}$ is defined to represent the desired manoeuvre trajectory. The detail of $\mathbf{y}_{des}$ will be discussed later. Then, the control input at each time step can be ascertained as the following steps.

The flight dynamics equation of Eq. (1) is transformed into

$$\dot{\mathbf{x}}(t_k)_m = \mathbf{f}(\mathbf{x}(t_k), u(t_k)_m) \tag{10}$$

where $t_k$ denotes the time step; $m$ represents the iteration step at the time point $t_k$. Therefore, the state vector at $t_{k+1}$ is obtained as follows

$$\mathbf{x}(t_{k+1})_m = \mathbf{x}(t_k) + \int_{t_k}^{t_{k+1}} \dot{\mathbf{x}}(t_k)dt \tag{11}$$

The trajectory of the tiltrotor $\mathbf{y}(t_{k+1})_m$ can be calculated from Eq. (11) and the flight dynamics model

$$\mathbf{y}(t_{k+1})_m = \mathbf{g}(\mathbf{x}(t_{k+1})_m, \mathbf{u}(t_k)_m) \tag{12}$$

Assume the tiltrotor is required to follow the desired trajectory $\mathbf{y}_{des}$. Then, Eq. (12) is used to form the error function

$$\mathbf{e}(t_{k+1})_m = \mathbf{y}(t_{k+1})_m - \mathbf{y}_{des}(t_{k+1}) \tag{13}$$

Combining Eqs. (10)-(12) with Eq. (13), the inverse simulation process can be symbolized as a "trim" at each time step. In other words, considering the dynamics characteristics of the flight dynamics model, the inverse simulation will search for the desired control strategy to ensure that the tiltrotor follows the given trajectory, $\mathbf{y}_{des}$. The corresponding objective function is the error vector, i.e., Eq. (13). This process is usually solved using the Newton-Raphson technique.

$$\mathbf{u}(t_k)_{m+1} = \mathbf{u}(t_k)_m - \mathbf{J}_m^{-1}\mathbf{e}(t_{k+1}) \tag{14}$$

where $\mathbf{J}_m$ is the Jacobian matrix describing the rate of change of the output vector with the control vector. Each element of the Jacobian matrix is given by

$$j_{i,j}(t_k)_m = \frac{\partial e_i(t_{k+1})_m}{\partial u_j(t_k)_m} \tag{15}$$

Numerical differentiation is widely used to calculate Eq. (15). However, this method has to execute the flight dynamics model repetitively, enlarging the time consumption. Estimates suggest that computation of the numerical differentiation occupies more than 75% of the overall time of the inverse simulation algorithm [12], making it challenging to improve its computational efficiency. Further, truncation errors are unavoidable using numerical differentiation, reducing the accuracy of the results. This would lead to additional calculation steps in the inverse simulation, which may further reduce the computational efficiency.

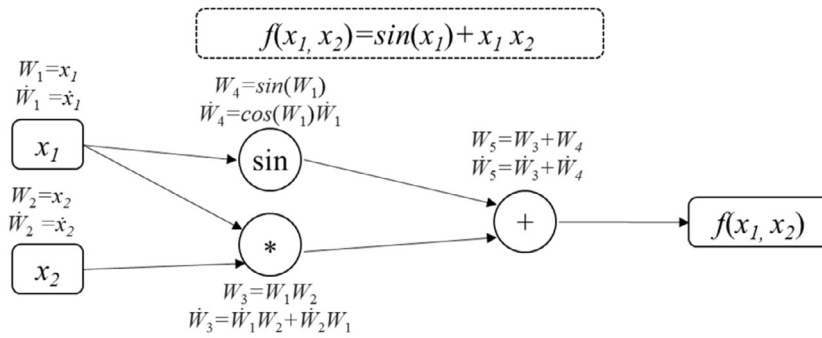### 2.3. Automatic differentiation method

The automatic differentiation (AD) method is based on the chain rule. This method removes repetitive calculations during the differentiation process and consequently reduces the time cost. It also avoids encountering the truncation errors derived from the numerical differentiation, thereby enhancing the precision of the Jacobian matrix. Full details of the AD method can be found in references [35].

Fig. 1 is utilised to illustrate the automatic differentiation method and its utilisation on the tiltrotor flight dynamics model.

The complicated equations inside the tiltrotor flight dynamics model can be decomposed into their constituent basic mathematical operations (addition, subtraction, etc.) and elementary functions (sin, cos, etc.), as shown in Fig. 1(a). Then, the chain rule is used to find the derivatives with respect to the independent variables. A simplified numerical example is shown in Fig. 1(b) to illustrate the automatic differentiation method. If the derivative of function $f$ to $x_1$ needs to be calculated at point $[x_1, x_2]$, $\dot{x}_1$ and $\dot{x}_2$ will be set to 1 and 0, respectively. Then, by computing and saving the value and the corresponding derivative of each node in the calculation process, the derivative ($\dot{W}_5$ in Fig. 1(b) example) can be automatically calculated using the chain rule. As can be seen in this calculation procedure, the automatic differentiation method avoids any truncation errors in the differentiation, enhancing the computational accuracy. Meanwhile, the derivative results can be obtained anytime without additional calculation, improving the efficiency. However, massive memory is needed to save calculation
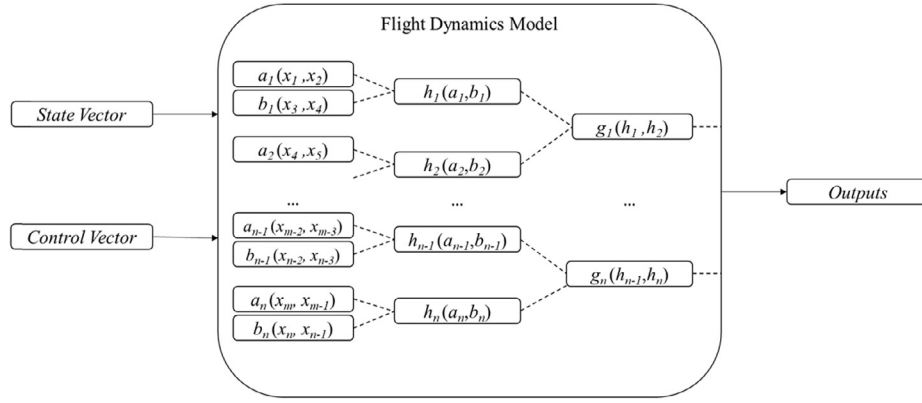
(a) Schematic Illustration of Flight Dynamics Model



(b) Simplified Example of the Automatic Differentiation (Forward Mode)

**Fig. 1.** Demonstration of the automatic differentiation method for flight dynamics modelling.

results at each node, which may cause additional time costs in the data transmission. This may become a potential risk impeding the utilisation of this method on massive computing tasks, such as CFD (Computational Fluid Dynamics) and FEA (Finite Element Analysis) calculations.

In this flight dynamics model, the FADBAD++ implementation [40] is introduced as the automatic differentiation library, and the forward mode of the automatic differentiation is adopted. The reason for choosing the forward mode is that the number of the inputs in the inverse simulation's differentiation process is similar to the number of the outputs, and the forward mode can improve the calculation efficiency in this case. Also, the tabular data in the flight dynamics model are replaced with high-order fitting polynomials to improve the differentiation accuracy. The calculation process of the AD embedded inverse simulation method can be concluded in Fig. 2, in which the red arrows represent the additional calculation steps when using the numerical differentiation method.

As indicated in Fig. 2, the flight dynamics model is called twice at each time step, rather than many times if the conventional numerical differentiation approach was implemented. This is because the numerical differentiation process needs to call the flight dynamics model whenever calculating derivative results. On the contrary, the AD method can obtain derivatives directly from the RAM. Therefore, significant improvement can be achieved in the computational efficiency of the inverse simulation approach. Meanwhile, as the tolerances (*tol*) of both methods are the same (1e-06), the accuracy improvement of the automatic differentiation method can reduce the iterations at each time step, further decreasing the time cost of the inverse simulation process.
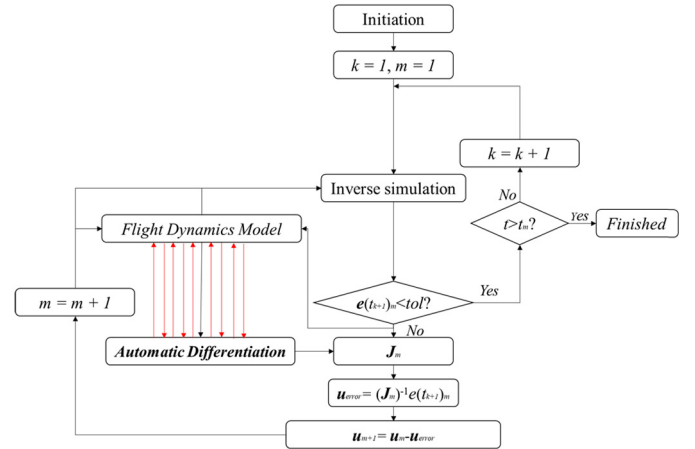


**Fig. 2.** Inverse simulation method integrated with automatic differentiation. (For interpretation of the colours in the figure(s), the reader is referred to the web version of this article.)

### 2.4. Mathematical description of the pop-up manoeuvre

This article utilises the pop-up manoeuvre to assess the accuracy and calculation efficiency of the proposed method as it has been utilised to evaluate the manoeuvrability of multiple rotorcraft configurations [41,42].

Fig. 3 represents an example of the pop-up manoeuvre, similar to the nap-of-the-earth (NOE) manoeuvre of rotorcraft. This manoeuvre assumes that the pilot's task is to clear an obstacle,
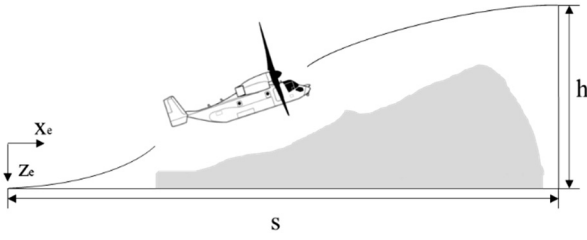
**Fig. 3.** The pop-up manoeuvre.

height $h$, over distance $s$. The impediment is located at the end of the manoeuvre.

The mathematical description of this manoeuvre is developed according to reference [38]. Firstly, the manoeuvre is executed in longitudinal and vertical degrees of freedom, and consequently, motions in the lateral and yawing channels will be disregarded. Therefore, the constraints in lateral and yawing directions are given as follows

$$\dot{\psi}(t) = 0 \tag{16}$$

$$\dot{y}_e(t) = 0 \tag{17}$$

where $\psi$ represents the yawing angle; $y_e$ denotes the lateral distance in the earth coordinate. The constraint of the altitude change ($z_e$) can be represented with a polynomial function shown as

$$z_e(t) = -h[6(\frac{t}{t_m})^5 - 15(\frac{t}{t_m})^4 + 10(\frac{t}{t_m})^3] \tag{18}$$

where $t_m$ is the time taken to complete the manoeuvre. Eq. (18) ensures the vertical velocity and vertical acceleration are fixed at zero at the beginning and end of this manoeuvre, and therefore the tiltrotor aircraft could achieve the required trajectory and guarantee the manoeuvre to be as smooth as possible. The longitudinal displacement $x_e$ can be evaluated numerically by integrating

$$\dot{x}_e(t) = \sqrt{V_{f,i}^2 - \dot{z}_e(t)^2} \tag{19}$$

where $V_{f,i}$ is the initial forward speed. Meanwhile, the vertical velocity, $\dot{z}_e$, is equal to zero at the beginning and end of the manoeuvre according to Eq. (18). Thus, the horizontal velocity $\dot{x}_e$ is equal to $V_{f,i}$ at these phases of the manoeuvre. The total horizontal track distance, $s$, is calculated as

$$s = \int_0^{t_m} \dot{x}_e(t) dt \tag{20}$$

Therefore, the time to complete the manoeuvre can be calculated using manoeuvre time $t_m$, track distance $s$, and initial forward speed $V_{f,i}$.

Eqs. (16)-(19) form four objective functions in this pop-up manoeuvre, and the "trim" objectives in the inverse simulation process are the four control inputs, namely, the collective pitch, the longitudinal controller, the lateral controller, and the pedal input.

## 3. Results and analysis

### 3.1. Validation of proposed inverse simulation method

The validation process is aimed to illustrate the accuracy of the improved inverse simulation method, and more importantly, to demonstrate the improvement of the calculation efficiency. The pertinent settings of the pop-up manoeuvre utilised in this section are shown in Table 1.
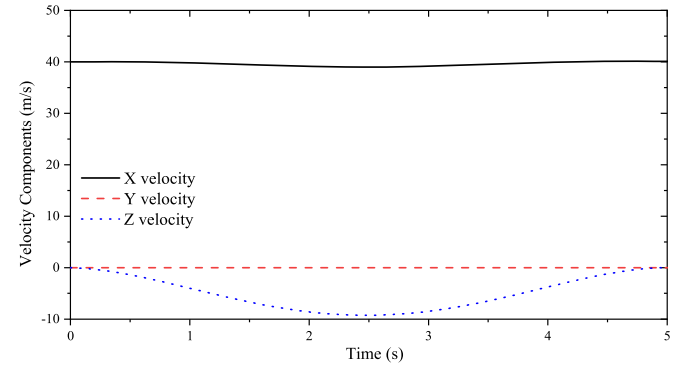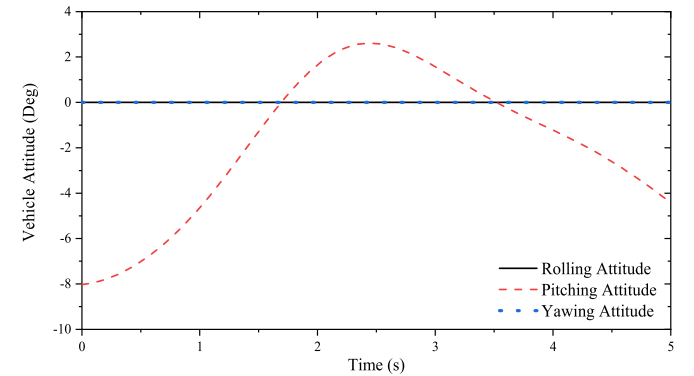
**Table 1**
Manoeuvre-related parameters.

| Parameters | Values |
| --- | --- |
| $s$ | 200 m |
| $V_{f,i}$ | 40 m/s |
| $h$ | 25 m |
| $t_m$ | 5.06 s |
| Nacelle angle | 0 deg (Helicopter mode) |
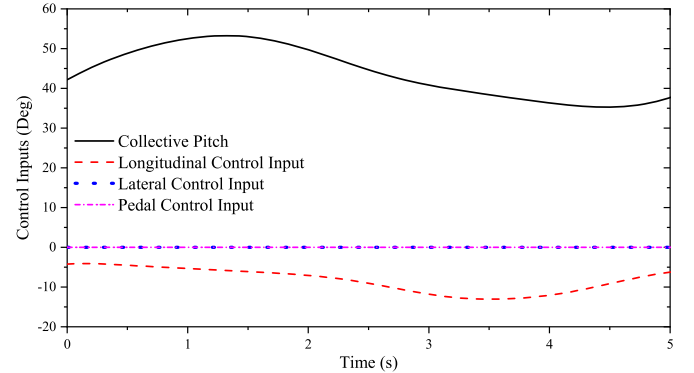


(a) Control Inputs



(b) Velocity Components in Earth Axis



(c) Vehicle Attitude

**Fig. 4.** Controls and states in pop-up manoeuvre.

Based on Table 1, the control action, the velocity components in the earth coordinate, and vehicle attitudes calculated by this inverse simulation method are shown in Fig. 4.

Due to the lack of pertinent flight tests or simulation results, the accuracy of the proposed inverse simulation method can only be verified by inspection and consideration of the underlying trends and features in the time histories.

The required collective pitch is influenced by the vertical acceleration involved in achieving the desired trajectory, as it controls the thrust of the tiltrotor. Meanwhile, the longitudinal control input remains at the trimmed value before 2.5 s. Then it increases
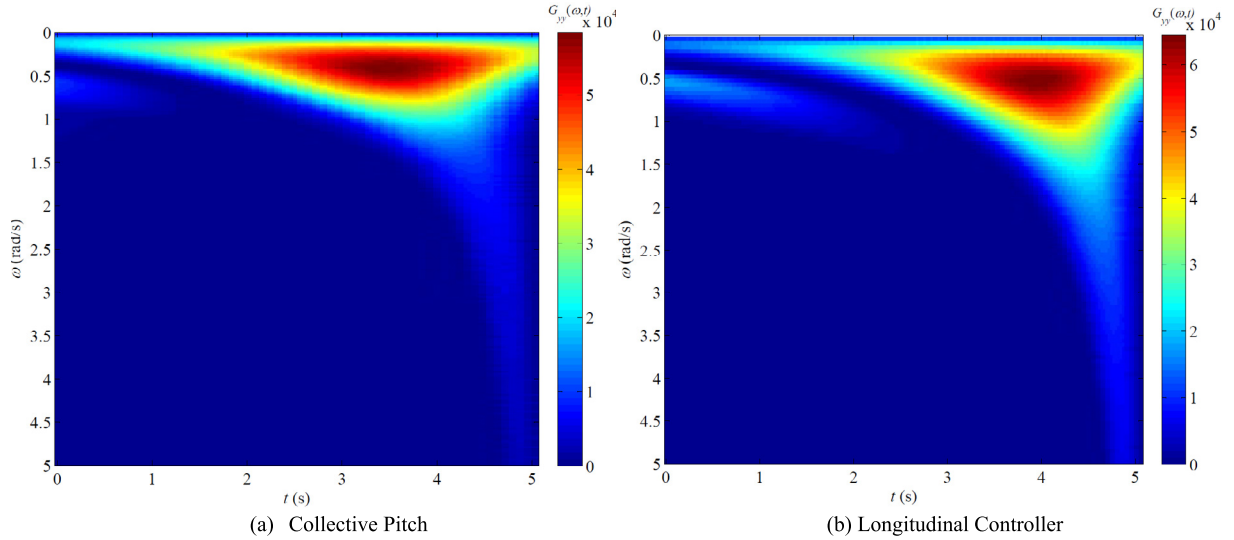
(a) Collective Pitch

(b) Longitudinal Controller

**Fig. 5.** Wavelet analysis for inverse simulation results.

and finally returns during the exit phase. Besides, the pitching attitude of the vehicle changes upwards at the beginning and moves downwards after 2.5 s. These phenomena arise because of the combined action of the rotor aerodynamics and flapping motion. Additionally, as the configuration of the tiltrotor aircraft is laterally symmetrical, the twin rotors are counter-rotating, and the pop-up manoeuvre is executed in longitudinal and vertical channels, there is no induced sidewards force or moment. Thus, the relevant trajectory description in the lateral and yawing channels, Eqs. (16)-(17), will ensure that lateral and pedal controls at zero across the manoeuvre.

Meanwhile, the pilot workload is analysed using the wavelet method [43,44], and the result is shown in Fig. 5.

According to Fig. 5, the main frequency ranges of the collective pitch and longitudinal controller are below 0.8 rad/s and 1.2 rad/s, respectively, suggesting that the pilot workloads in both control inputs are relatively low. Therefore, handling quality ratings of collective pitch and longitudinal controller are in Level 1 and Level 2, according to reference [45].

Furthermore, the efficiency of the proposed inverse simulation method is also assessed. The calculation is executed on the platform with a 12-cores base speed 3.80 GHz CPU and 16G RAM without using the parallel computing method. The time normalisation method is defined as follows

$$\bar{t} = \frac{t_{cal}}{t_{real}} \times 100\% \tag{21}$$

where $t_{cal}$ is the calculation time, and $t_{real}$ denotes the corresponding real-time cost. The normalisation time cost of the obtained inverse simulation process is shown in Table 2. The time cost is also dependent on the initial setting, CPU temperature, and other issues. Therefore, the inverse simulation process is implemented several times to obtain its minimum, maximum, and average time cost results. The inverse simulation time cost with the numerical differentiation method is also added to Table 2 as a comparison.

According to Table 2, the calculation time is lower than the real-time period using the automatic differentiation method, indicating that the proposed inverse simulation could achieve the faster-than-realtime capability. The time cost using the numerical differentiation method is a little more than eight times larger than the cost using the automatic differentiation method. There are four trim objectives in the inverse simulation process. Therefore, the

**Table 2**
Calculation efficiency evaluation of the proposed inverse simulation method.

|  | Automatic differentiation method | Numerical differentiation method |
|---|---|---|
| Min | 76% | 616% |
| Max | 91% | 805% |
| Avg | 83% | 693% |

flight dynamics model needs to be called 16 times when using the numerical differentiation method, rather than only twice using the automatic differentiation method. On the other hand, the accuracy improvement due to the AD method can also improve computational efficiency. The AD method would provide a more accurate Jacobian matrix and may reduce the calculation iteration steps. This would further reduce the time cost of the inverse simulation process.

### 3.2. Manoeuvrability analysis for tiltrotor aircraft

With the proposed inverse simulation method, the manoeuvrability analysis of the tiltrotor aircraft can be expanded into various flight states easily, including different forward speeds, track distances, and nacelle incidence angles. When executing the pop-up manoeuvre at various forward speeds, control action results are shown in Fig. 6, where nacelle incidence is fixed at zero (helicopter mode), and the track distance is set to 200 m. Furthermore, the relevant handling qualities and normalisation time cost are shown in Table 3.

As shown in Fig. 6, the forward speed influences the control input during the pop-up manoeuvre. The increase of the forward speed leads to additional aggressiveness and reduces the handling quality. According to the setting of the pop-up manoeuvre, the manoeuvre duration is determined by the forward speed. When the speed decreases, the tiltrotor aircraft requires more time to achieve this manoeuvre, consequently reducing aggressiveness. Furthermore, Fig. 6 also indicates the similarity of the control strategies at various flight speeds. The control strategies in different control channels share similar trends. Also, the faster-than-realtime capability can be satisfied at different forward speeds.

Fig. 7 shows inverse simulation results with different track distances, where the nacelle incidence angle is fixed at zero, and the initial forward speed is 40 m/s. Further, the relevant handling quality ratings and the normalisation time cost are shown in Table 4.
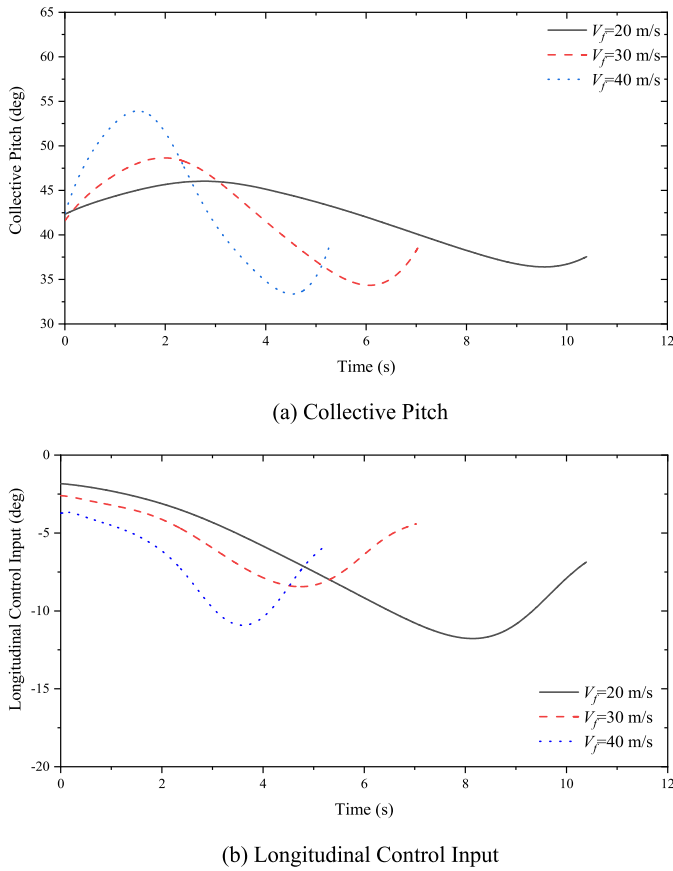
(a) Collective Pitch



(a) Collective Pitch



(b) Longitudinal Control Input

**Fig. 6.** Inverse simulation results with forward speeds.



(b) Longitudinal Control Input

**Fig. 7.** Inverse simulation results with different track distances.

**Table 3**
Handling quality ratings and calculation efficiency in different forward speeds.

| Initial forward speed (m/s) | Ratings (collective pitch) | Ratings (longitudinal control) | Normalisation time cost |
|---|---|---|---|
| 20 | Level 1 | Level 1 | 85% |
| 30 | Level 1 | Level 1 | 84% |
| 40 | Level 1 | Level 2 | 83% |

**Table 4**
Handling quality ratings and calculation efficiency in different track distances.

| Track distance (m) | Ratings (collective pitch) | Ratings (longitudinal control) | Normalisation time cost |
|---|---|---|---|
| 200 | Level 1 | Level 2 | 83% |
| 300 | Level 1 | Level 1 | 79% |
| 500 | Level 1 | Level 1 | 75% |
| 800 | Level 1 | Level 1 | 69% |

Fig. 7 and Table 4 demonstrate the inverse simulation results, pertinent handling quality ratings, and normalisation time costs with different track distances. As the track distance increases, the aggressiveness of the control input drops down, indicating improved handling qualities. A longer track distance corresponds to more time to finish this manoeuvre. Once the track distance is set to be 800 m, the control action roughly remains at the trimmed value, indicating that the pilot workload is relatively low during this manoeuvring flight. Moreover, the normalisation time costs decrease with increasing track distances and are all lower than 100%, showing that the proposed method can achieve faster-than-realtime performance in different track distance settings.

Fig. 8 shows the control inputs of the collective pitch and the longitudinal control input with different nacelle incidence angles, with the track distance of 200 m, initial forward speed at 40 m/s. The handling quality ratings and the normalisation time cost are depicted in Table 5.

According to Fig. 8, the nacelle angle plays a critical role in the control strategies for the tiltrotor aircraft to achieve the pop-up manoeuvre. The handling quality ratings in both control inputs become worse by tilting forward the nacelle. According to the control strategy of the tiltrotor aircraft, the control allocation between the longitudinal cyclic pi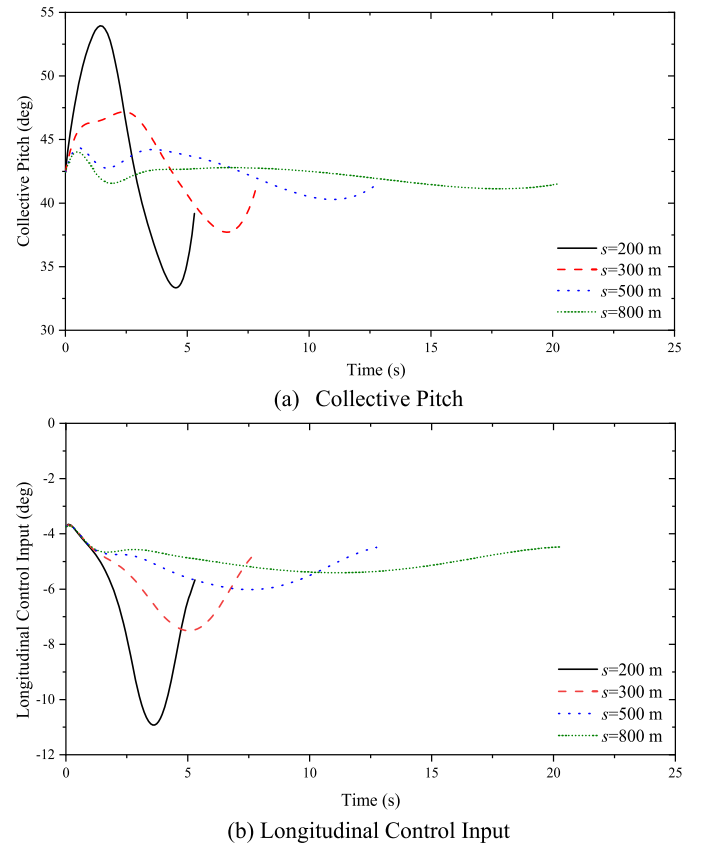tch and the elevator deflection is determined by the nacelle incidence angle. However, the control power of the elevator is relatively low when the forward speed is 40 m/s. It causes the overall longitudinal control power to be reduced, leading to an additional change in longitudinal control input.

On the other hand, when the nacelle is tilted forward, the collective pitch can not only alter the vertical acceleration but also change the propulsive force. It further complicates the flight dynamics characteristics. Moreover, the pop-up manoeuvre is widely used in helicopter manoeuvrability analysis, but it may be inappropriate for fixed-wing aircraft or even the tiltrotor in the conversion mode. The altitude change $h$ is directly described in this manoeuvre, and the collective pitch in helicopter mode can provide the associated vertical acceleration. However, the fixed-wing aircraft cannot directly control the altitude like rotorcraft due to the non-minimum phase characteristics [46]. Thus, the manoeuvrability of the tiltrotor aircraft in this manoeuvre declines as nacelle incidence increases.

Based on Table 5, the time costs are lower than 100% with different nacelle incidence angles. Therefore, the improved inverse simulation method satisfies the faster-than-realtime requirement at multiple flight states and manoeuvre settings.

Thanks to the efficiency improvement of the proposed inverse simulation method, the manoeuvrability at different flight states can be calculated in a relatively short time. Thus, the velocity-
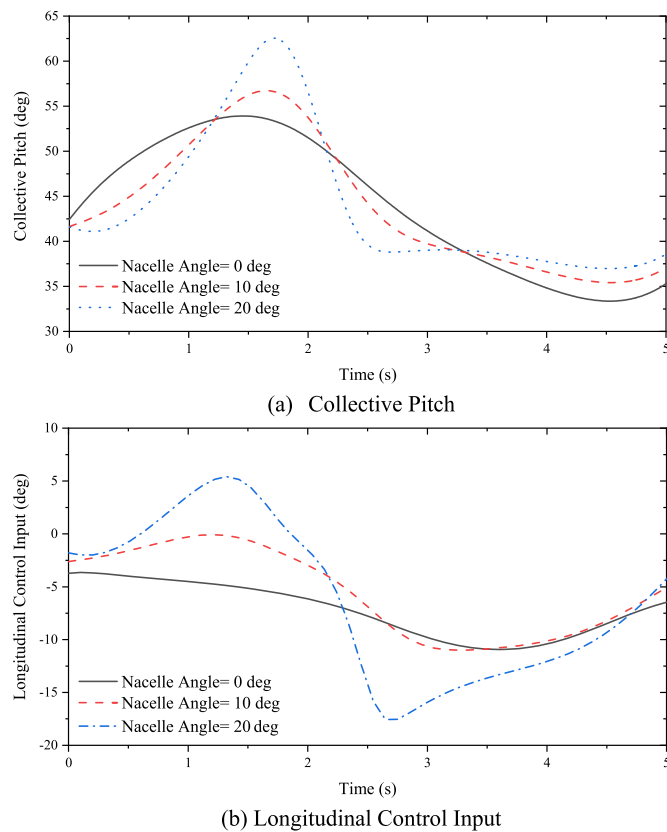
(a) Collective Pitch



(b) Longitudinal Control Input

**Fig. 8.** Inverse simulation results with different nacelle incidence angles.

**Table 5**
Handling quality ratings and calculation efficiency in different nacelle incidence angles.

| Nacelle incidence angle (deg) | Ratings (collective pitch) | Ratings (longitudinal control) | Normalisation time cost |
|---|---|---|---|
| 0 | Level 1 | Level 2 | 83% |
| 10 | Level 2 | Level 2 | 85% |
| 20 | Level 3 | Level 3 | 86% |

nacelle incidence envelope that could safely achieve the pop-up manoeuvre is calculated in Fig. 9, where track distance $s = 200$ m. The grey area is the region that the XV-15 tiltrotor aircraft can perform the pop-up manoeuvre. This envelope is determined by two factors. First, the inverse simulation results can be achieved across the manoeuvre; second, the corresponding handling qualities should at least satisfy the Level 3 requirement. Meanwhile, the conversion corridor (within this envelope, the tiltrotor can fly safely) of the XV-15 tiltrotor aircraft [47] is also added in Fig. 9 as a comparison.

As represented in Fig. 9, the speed range where the pop-up manoeuvre can be achieved is dependent on the nacelle incidence angle and forward speed. When the tiltrotor aircraft is in helicopter mode, this range is close to its flight envelope. However, when the nacelle is tilted forward, the upper limit of the manoeuvring envelope is significantly reduced. The non-minimum phase characteristics due to tilting forward the nacelle angles impede the pop-up manoeuvre from being performed. On the other hand, the lower limit of this manoeuvre envelope is close to the conversion envelope. When the initial speed is relatively small, the aggressiveness in the pop-up manoeuvre is significantly reduced. The capability to obtain the trim state would be the most critical challenge at this flight range.
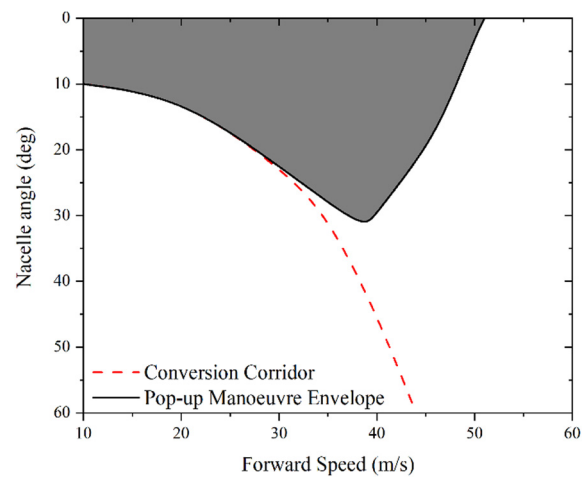


**Fig. 9.** Velocity-nacelles incidence envelope for pop-up manoeuvre for XV-15 tiltrotor.

## 4. Conclusion

A new inverse simulation method has been developed incorporating the automatic differentiation method and tiltrotor flight dynamics model. The pop-up manoeuvre is utilised to assess the performance of the improved inverse simulation method and the manoeuvrability and handling qualities of the tiltrotor aircraft at different flight states. The main conclusions from the current work are as follows:

1) According to the inverse simulation results of the pop-up manoeuvre, obtained control inputs follow the understood flight dynamics characteristics of the tiltrotor aircraft, which gives confidence in the likely accuracy of these results.
2) The fast-than-realtime capability of the proposed inverse simulation method is verified in different flight states, allowing this method to assist relevant autonomous system design, especially having the potential to be introduced into the autopilot system design.
3) The pop-up manoeuvre results indicate that the growth of nacelle angle and forward speed impedes the aircraft to finish this manoeuvre safely. The handling qualities are also dependent on the track distance of the manoeuvre. Meanwhile, the velocity-nacelle incidence envelope to perform the pop-up manoeuvre safely is obtained using the proposed inverse simulation method to demonstrate these influences further.

### Declaration of competing interest

The authors declare the following financial interests/personal relationships which may be considered as potential competing interests: Ye Yuan, David Anderson, Douglas Thomson reports financial support was provided by Engineering and Physical Sciences Research Council grant EP/S013814/1.

## References

[1] A. Jimenez Garcia, G.N. Barakos, Numerical simulations on the ERICA tiltrotor, Aerosp. Sci. Technol. 64 (2017) 171–191, https://doi.org/10.1016/j.ast.2017.01.023.

[2] G.D. Padfield, M.D. White, Flight simulation in academia HELIFLIGHT in its first year of operation at the University of Liverpool, Aeronaut. J. 107 (2003) 529–538, https://doi.org/10.1017/S0001924000013415.

[3] W. Staruk, A. Datta, Fundamental understanding, prediction, and validation of tiltrotor dynamic loads in transition flight using RANS/FEA, in: 58th AIAA/ASCE/AHS/ASC Struct. Struct. Dyn. Mater. Conf. 2017, 2017, pp. 1–22.

[4] K. Lu, C. Liu, C. Li, R. Chen, Flight dynamics modeling and dynamic stability analysis of tilt-rotor aircraft, Int. J. Aerosp. Eng. 2019 (2019) 1–15, https://doi.org/10.1155/2019/5737212.

[5] W. Wu, R. Chen, An improved online system identification method for tiltrotor aircraft, Aerosp. Sci. Technol. 110 (2021) 106491, https://doi.org/10.1016/j.ast.2021.106491.

[6] X. Yan, R. Chen, Augmented flight dynamics model for pilot workload evaluation in tilt-rotor aircraft optimal landing procedure after one engine failure, Chin. J. Aeronaut. 32 (2019) 92–103, https://doi.org/10.1016/j.cja.2018.06.010.

[7] J.F. Tan, T.Y. Zhou, Y.M. Sun, G.N. Barakos, Numerical investigation of the aerodynamic interaction between a tiltrotor and a tandem rotor during shipboard operations, Aerosp. Sci. Technol. 87 (2019) 62–72, https://doi.org/10.1016/j.ast.2019.02.005.

[8] G. Di Francesco, M. Mattei, Modeling and incremental nonlinear dynamic inversion control of a novel unmanned tiltrotor, J. Aircr. 53 (2016) 73–86, https://doi.org/10.2514/1.C033183.

[9] C. Papachristos, K. Alexis, A. Tzes, Hybrid model predictive flight mode conversion control of unmanned Quad-TiltRotors, in: 2013 Eur. Control Conf. ECC 2013, 2013, pp. 1793–1798.

[10] S. Yanguo, W. Huanjin, Design of flight control system for a small unmanned tilt rotor aircraft, Chin. J. Aeronaut. 22 (2009) 250–256, https://doi.org/10.1016/S1000-9361(08)60095-3.

[11] K. Ferguson, D. Thomson, Examining the stability derivatives of a compound helicopter, Aeronaut. J. 121 (2017) 1–20, https://doi.org/10.1017/aer.2016.101.

[12] D. Thomson, R. Bradley, Inverse simulation as a tool for flight dynamics research—principles and applications, Prog. Aerosp. Sci. 42 (2006) 174–210, https://doi.org/10.1016/j.paerosci.2006.07.002.

[13] Y. Yuan, D. Thomson, R. Chen, Variable rotor speed strategy for coaxial compound helicopters with lift-offset rotors, Aeronaut. J. 124 (2020) 96–120, https://doi.org/10.1017/aer.2019.113.

[14] D.G. Thomson, R. Bradley, The principles and practical application of helicopter inverse simulation, Simul. Pract. Theory 6 (1998) 47–70, https://doi.org/10.1016/S0928-4869(97)00012-8.

[15] A. Güneş Baydin, B.A. Pearlmutter, A. Andreyevich Radul, J. Mark Siskind, Automatic differentiation in machine learning: a survey, J. Mach. Learn. Res. 18 (2018) 1–43.

[16] J.D. Hodson, D.F. Hunsaker, R.E. Spall, Wing optimization using dual number automatic differentiation in MachUp, in: AIAA SciTech Forum - 55th AIAA Aerosp. Sci. Meet., 2017.

[17] Z. Lyu, G.K.W. Kenway, C. Paige, J.R.R.A. Martins, Automatic differentiation adjoint of the Reynolds-averaged Navier-Stokes equations with a turbulence model, in: 21st AIAA Comput. Fluid Dyn. Conf., 2013, pp. 1–24.

[18] J.P. Thomas, E.H. Dowell, K.C. Hall, Using automatic differentiation to create a nonlinear reduced-order-model aerodynamic solver, AIAA J. 48 (2010) 19–24, https://doi.org/10.2514/1.36414.

[19] F.F. Felker, M.D. Maisel, M.D. Betzina, Full-scale tilt-rotor hover performance, J. Am. Helicopter Soc. 31 (1986) 10–18, https://doi.org/10.4050/JAHS.31.2.10.

[20] S.W. Ferguson, A Mathematical Model for Real Time Flight Simulation of a Generic Tilt-Proprotor Aircraft, NASA CR 166536, 1988.

[21] G.L. Ghiringhelli, P. Masarati, P. Mantegazza, M.W. Nixon, Multi-body analysis of the 1/5 scale wind tunnel model of the V-22 tiltrotor, in: Annu. Forum Proc. - Am. Helicopter Soc., vol. 1, 1999, pp. 1087–1096.

[22] W. Koning, Wind Tunnel Interference Effects on Tiltrotor Testing Using Computational Fluid Dynamics, NASA CR 219086, 2016, http://www.sti.nasa.gov.

[23] R.L. Marr, W.E.B. Roderick, Handling qualities evaluation of the XV-15 tilt rotor aircraft, J. Am. Helicopter Soc. 20 (1975) 23–33, https://doi.org/10.4050/JAHS.20.23.

[24] E. Gires, Simulation framework for civil tiltrotor mission performance, Int. J. Eng. Technol. 7 (2018) 178–187, https://doi.org/10.14419/ijet.v7i4.13.21352.

[25] B.M. Kim, B.S. Kim, N.W. Kim, Trajectory tracking controller design using neural networks for a tiltrotor unmanned aerial vehicle, Proc. Inst. Mech. Eng., Part G, J. Aerosp. Eng. 224 (2010) 881–896, https://doi.org/10.1243/09544100JAERO710.

[26] S. Rutherford, D.G. Thomson, Helicopter inverse simulation incorporating an individual blade rotor model, J. Aircr. 34 (1997) 627–634, https://doi.org/10.2514/2.2239.

[27] S. Rutherford, D.G. Thomson, Improved methodology for inverse simulation, Aeronaut. J. 100 (1996) 79–85, https://doi.org/10.1017/S0001924000067348.

[28] N. Cameron, D.G. Thomson, D.J. Murray-Smith, Pilot modelling and inverse simulation for initial handling qualities assessment, Aeronaut. J. 107 (2003) 511–520.

[29] W. Wu, A general method for closed-loop inverse simulation of helicopter maneuver flight, Chin. J. Aeronaut. 30 (2017) 1799–1808, https://doi.org/10.1016/j.cja.2017.07.010.

[30] Y. Yuan, D. Thomson, R. Chen, Investigation of lift offset on flight dynamics characteristics for coaxial compound helicopters, J. Aircr. 56 (2019) 2210–2222, https://doi.org/10.2514/1.C035190.

[31] Y. Yuan, D. Thomson, D. Propeller design to improve flight dynamics features and performance for coaxial compound helicopters, Aerosp. Sci. Technol. 106 (2020) 106096, https://doi.org/10.1016/j.ast.2020.106096.

[32] Y. Yuan, R. Chen, P. Li, Trim investigation for coaxial rigid rotor helicopters using an improved aerodynamic interference model, Aerosp. Sci. Technol. 85 (2019) 293–304, https://doi.org/10.1016/j.ast.2018.11.044.

[33] R. Chen, Y. Yuan, D. Thomson, A review of mathematical modelling techniques for advanced rotorcraft configurations, Prog. Aerosp. Sci. 120 (2021) 100681, https://doi.org/10.1016/j.paerosci.2020.100681.

[34] S. Ferguson, Development and Validation of a Simulation for Generic Tilt-Rotor Aircraft, NASA-CR-166537, 1989.

[35] Y. Yuan, D. Thomson, D. Anderson, Application of automatic differentiation for tilt-rotor aircraft flight dynamics analysis, J. Aircr. 57 (2020) 985–990, https://doi.org/10.2514/1.C035811.

[36] G.D. Padfield, Helicopter Flight Dynamics, John Wiley & Sons, Ltd, Chichester, UK, 2018.

[37] K. Ferguson, D. Thomson, Maneuverability assessment of a compound helicopter configuration, J. Am. Helicopter Soc. 61 (2016) 1–15, https://doi.org/10.4050/JAHS.61.012008.

[38] D.G. Thomson, R. Bradley, The use of inverse simulation for preliminary assessment of helicopter handling qualities, Aeronaut. J. 101 (1997) 287–294, https://doi.org/10.1017/S0001924000066148.

[39] Y. Yuan, D. Thomson, R. Chen, R. Dunlop, Heading control strategy assessment for coaxial compound helicopters, Chin. J. Aeronaut. 32 (2019) 2037–2046, https://doi.org/10.1016/j.cja.2019.04.008.

[40] C. Bendtsen, O. Stauning, FADBAD, a flexible C++ package for automatic differentiation, Dep. Math. Model. Technical University of Denmark, 1996, http://www2.imm.dtu.dk/~kajm/FADBAD/tr17_96.pdf.

[41] M.E. Rosti, M. Omidyeganeh, A. Pinelli, Numerical simulation of a passive control of the flow around an aerofoil using a flexible, self adaptive flaplet, Flow Turbul. Combust. 100 (2018) 1111–1143, https://doi.org/10.1007/s10494-018-9914-6.

[42] Y. Yuan, D. Thomson, D. Anderson, Manoeuvrability investigation for tiltrotor aircraft with an integrated simulation engine, in: 47th Eur. Rotorcr. Forum, 2021, pp. 1–9.

[43] L. Lu, M. Jump, M. Jones, Tau coupling investigation using positive wavelet analysis, J. Guid. Control Dyn. 36 (2013) 920–934, https://doi.org/10.2514/1.60015.

[44] J.G. Jones, G.D. Padfield, M.T. Charlton, Wavelet analysis of pilot workload in helicopter low-level flying tasks, Aeronaut. J. 103 (1999) 55–63, https://doi.org/10.1017/S0001924000065106.

[45] J.K. Tritschler, J.C. O'Connor, J.A. Pritchard, R. Wallace, Exploratory investigation into rotorcraft pilot strategy and visual cueing effects in the shipboard environment, J. Am. Helicopter Soc. 65 (2020) 1–13, https://doi.org/10.4050/JAHS.65.022003.

[46] J. Hauser, S. Sastry, G. Meyer, Nonlinear control design for slightly non-minimum phase systems: application to V/STOL aircraft, Automatica 28 (1992) 665–679, https://doi.org/10.1016/0005-1098(92)90029-F.

[47] M.D. Maisel, D.J. Giulianetti, D.C. Dugan, The History of the XV-15 Tilt Rotor Research Aircraft: From Concept to Flight, 2000.